scientific reports

Check for updates

OPEN

Micro-structural investigations on oppositely charged mixed surfactant gels with potential dermal applications

Manas Barai[1], Emili Manna[2], Habiba Sultana[1], Manas Kumar Mandal[1], Kartik Chandra Guchhait[3], Tuhin Manna[3], Anuttam Patra[4], Chien-Hsiang Chang[5], Parikshit Moitra[6], Chandradipa Ghosh[3], Anna-Carin Larsson[4], Santanu Bhattacharya[6,7] & Amiya Kumar Panda[1]✉

Dicarboxylic amino acid-based surfactants (*N*-dodecyl derivatives of -aminomalonate, -aspartate, and -glutamate) in combination with hexadecyltrimethylammonium bromide (HTAB) form a variety of aggregates. Composition and concentration-dependent mixtures exhibit liquid crystal, gel, precipitate, and clear isotropic phases. Liquid crystalline patterns, formed by surfactant mixtures, were identified by polarizing optical microscopy. FE-SEM studies reveal the existence of surface morphologies of different mixed aggregates. Phase transition and associated weight loss were found to depend on the composition where thermotropic behaviours were revealed through combined differential scanning calorimetry and thermogravimetric studies. Systems comprising more than 60 mol% HTAB demonstrate shear-thinning behaviour. Gels cause insignificant toxicity to human peripheral lymphocytes and irritation to bare mouse skin; they do not display the symptoms of cutaneous irritation, neutrophilic invasion, and inflammation (erythema, edema, and skin thinning) as evidenced by cumulative irritancy index score. Gels also exhibit substantial antibacterial effects on *Staphylococcus aureus*, a potent causative agent of skin and soft tissue infections, suggesting its possible application as a vehicle for topical dermatological drug delivery.

Formation of gels and different liquid crystalline phases by oppositely charged mixed surfactant systems depend on the composition, surfactant chain length, salinity, temperature, pH and external field, etc.[1–5]. Artificial gels possess regulated super-structure[6–10], where the properties of the fabricated liquid crystals depend on electrostatic, hydrogen bond, hydrophobic, and van der Waals interactions among the components[11–13]. Gels are associated with two independent transitions, viz., the sol–gel transition of the gelator and anisotropic-isotropic transition of the liquid crystals[9,10,14–18]. Gelatinous property, structure, and shape of surfactant aggregates largely depend on the molecular architecture of the aggregating species[14,19,20].

Gels have versatile applications in tissue engineering[21], hemostasis bandages[22–26], photo-patterning[17,27–30], 3D-printing[31,32], electrochemistry[33], pharmaceutical formulation[5,34–36], and regenerative medicine[10,37–39], etc. Recent advances in the design and synthesis of dicarboxylic amino acid-based surfactants (AAS) have opened up their wide range of applications as chelator in metal extraction[40]. Due to its "green nature", aggregation behaviour of AAS in combination with HTAB have been studied in detail where some mixed surfactants can form gel[16]. This has encouraged the present research group to undertake further investigations on such aggregates at higher concentrations to explore the possibility of using those for topical dermatological drug delivery.

The main aim of the present work is to undertake physicochemical investigations on different types of aggregates formed by AAS + HTAB. While HTAB shows antimicrobial activities, AASs are biocompatible[41]. Because

[1]Department of Chemistry, Vidyasagar University, Midnapore 721102, West Bengal, India. [2]Centre for Life Sciences, Vidyasagar University, Midnapore 721102, West Bengal, India. [3]Department of Human Physiology, Vidyasagar University, Midnapore 721102, West Bengal, India. [4]Chemistry of Interfaces Group, Luleå University of Technology, 97187 Luleå, Sweden. [5]Department of Chemical Engineering, National Cheng Kung University, Tainan, Taiwan. [6]India and School of Applied & interdisciplinary Sciences, Indian Association for the Cultivation of Science, Kolkata 700032, India. [7]Department of Organic Chemistry, Indian Institute of Science, Bangalore 560012, Karnataka, India. ✉email: akpanda@mail.vidyasagar.ac.in

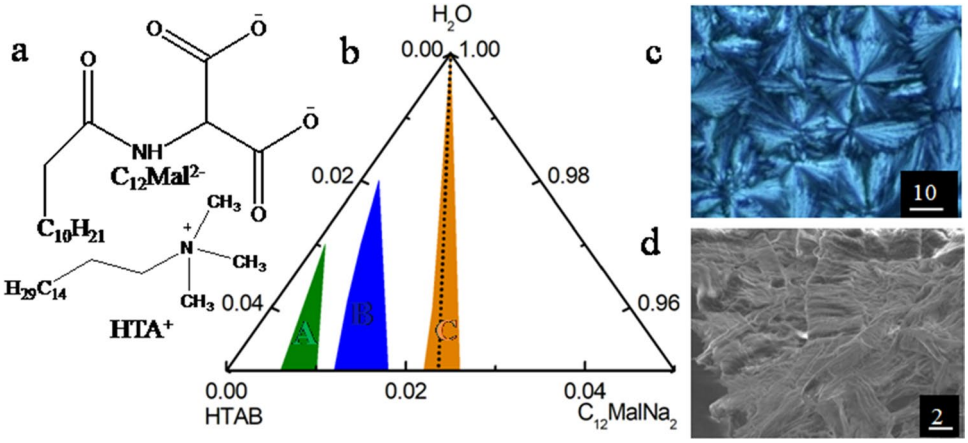

Figure 1. (**a**) Chemical structure of $C_{12}Mal^{2-}$ and HTA^+; (**b**) truncated phase diagram of $C_{12}MalNa_2$ + HTAB + water mixed system at 25 °C. Phases: (A), gel; (B), viscous; (C), precipitate; and clear region indicate the formation of micelle. The dotted line in panel b corresponds to equimolar region. Panel (**c**), POM and (**d**), FE-SEM image of 5 wt% $C_{12}MalNa_2$ + HTAB (40:60, *w*/*w*) gel respectively. Scale bars (in μm) are mentioned in the microscopic images.

of its toxicity, individual use of HTAB is unwarranted. It is believed that, when HTAB is used in combination with AASs, its toxicity will be substantially reduced[42,43]. To check the biocompatibility of gels and their possible dermatological application in the topical form, cytotoxicity, skin irritation, and histological studies were carried out. HTAB is known to have antimicrobial activities[42], for which antibacterial activities of AAS + HTAB mixtures are considered to be worth investigating. Hence, antibacterial activities of the gels on *Staphylococcus aureus*, one of the causative agents for persistent skin and soft tissue infections, were also explored.

Results and discussion

Structures of $C_{12}MalNa_2$ and HTAB are shown in (Fig. 1a) along with other information. Manifestation on the Gibbs ternary phase diagram (Fig. 1b) demonstrates the occurrence of gel, viscous, precipitate and clear fluid states. With increasing proportion of HTAB, surfactant mixtures form gels where the relative proportion of viscous and gel states increase following the order: $C_{12}MalNa_2$ + HTAB > $C_{12}AspNa_2$ + HTAB > $C_{12}GluNa_2$ + HTAB (Fig. S1, supplementary section). Hydrophobic interaction between AASs and HTAB is the predominant factor for the formation of different types of aggregates besides the electrostatic attraction[8]. AASs interact with HTAB at a 1:2 mol ratio and form gels at equimolar region due to the dominance of the HTAB molecules[44]. Microstructural investigations on surfactant mixtures at different concentrations (AAS + HTAB) and different compositions (AAS/HTAB) were further investigated through polarizing optical microscopy (POM) and field emission scanning electron microscopic (FE-SEM) studies. POM studies reveal the occurrence of liquid crystal and associated textures as shown in Fig. 1c. Gels exhibit different textures in the surfactant concentration range of 3–5 wt%. With increasing proportions of HTAB, $C_{12}MalNa_2$ + HTAB gels display nematic, smectic, spherulite, cholesteric, calamitic, and flower-like textures (Fig. S2, Table S1A)[44–47]. Nematic liquid textures originate from thread-like shapes, that correspond to surfactant gels aligning themselves in threadlike shapes as reported earlier[48]. The patterns become more complex with enhanced sizes due to the aggregation and associative interactions between AASs and HTAB. Texture size increases with increasing proportions of HTAB, which has a higher cross-sectional area than the AASs[49].

Features become more prominent with increasing mixed surfactant concentrations, common in the case of lyotropic liquid crystals[16,47] (Fig. S2, Supplementary Section). In the case of $C_{12}AspNa_2$ + HTAB gels for 50, 60, and 80 wt% of HTAB, smectic (Fig. S3a_1), spherulite (Fig. S3b_1), and flower-like (Fig. S3c_1) patterns are observed[50,51], while in the case of $C_{12}GluNa_2$ + HTAB mixtures, discotic (Fig. S3a_2), calamitic (Fig. S3b_2), and flower-like (Fig. S3c_2, Table S1B) textures are observed due to the formation of sterically favourable seven and eight-member rings. Two carboxylate groups get progressively separated by one methylene group while moving from $C_{12}MalNa_2$ to $C_{12}AspNa_2$ to $C_{12}GluNa_2$. Accordingly, two carboxylate groups of AASs can electrostatically interact with one HTAB to form six, seven, and eight-member rings[49]. Smectic textures designate ordered and rigid layer structure whereby $C_{12}MalNa_2$ + HTAB can closely interact with HTAB to exhibit smectic textures (Fig. S2b_1,c_2,a_4,c_4). The nematic texture (Fig. S2a_1,b_2,a_3), is characteristic of stacked layer and positional order whereby the discotic texture (Fig. S2b_4) is due to rigid disk-like core, according to Fan Shao et al.[52,53]. Spherulite textures (Fig. S2a_5 and b_3) are larger bundles and the hexagonal shapes caused by close packing are even more defined, as also reported by Haas et al.[54] $C_{12}MalNa_2$ + HTAB gels display a more prominent spherulite texture (Fig. S2a_5,b_3) than $C_{12}AspNa_2$ + HTAB due to the formation of strongly aggregated structure and associative interaction with HTAB. Calamitic textures, exhibited by $C_{12}GluNa_2$ + HTAB gels (Fig. S3b_2, Table S1B) have a relatively flexible core, due to weak hydrophobic interaction between the oppositely charged $C_{12}GluNa_2$ and HTAB system.

Microstructures of the aggregates were further investigated with FE-SEM studies, which display interconnected morphologies (Fig. 1d)[27,55,56]. To achieve optimal solvation and swelling, the pore of the gels can provide

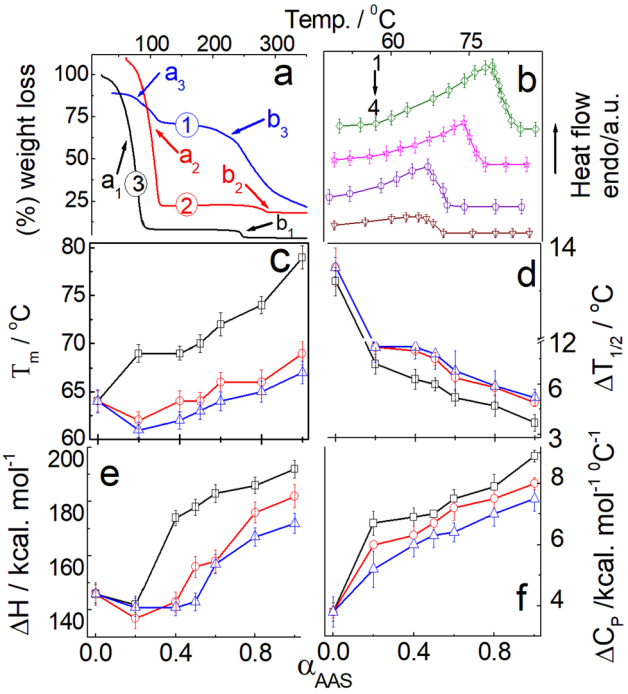

Figure 2. (**a**) TGA of AAS + HTAB (100 mM, 40/60, M/M) gel. Systems: 1, $C_{12}GluNa_2$ + HTAB; 2, $C_{12}AspNa_2$ + HTAB and 3, $C_{12}MalNa_2$ + HTAB. a_1, b_1, a_2, b_2, a_3, and b_3 represent different phase transitions. (**b**) DSC of $C_{12}MalNa_2$ + HTAB mixture at different mole% of $C_{12}MalNa_2$: 1, 80; 2, 60; 3, 40 and 4, 0. Variations of (**c**) chain melting temperature (T_m); (**d**) half peak height ($\Delta T_{1/2}$); (**e**) enthalpy change (ΔH) and (**f**) heat capacity change (ΔC_p) with the mole fraction of AAS (α_{AAS}). The line colours in panels (**c**–**f**) represent similar surfactant composition as in panel (**a**). Scan rate: 2 °C min^{-1}.

pockets for water molecules, necessary for hydration, to be included by surface tension. $C_{12}MalNa_2$, in combination with HTAB, shows flower-like (Fig. S4e_1,b_4,b_5,c_5,e_5 and Table S1A), coral-like (Fig. S4a_1,d_2), and porous—(Fig. S4a_3) architectures due to the existence of protrusions and larger channels[57]. Flake—(Fig. S4c_1,b_3,c_4), leaf—(Fig. S4b_1,d_1,a_2), leaf + flake—(Fig. S4b_2), wrinkled—(Fig. S4a_5), and sheet-like structures (Fig. S4d_3) display extended flat features. Fibrous texture (Fig. S4c_3 and d_5) indicate larger bundled-fibre network structure. Granular—(Fig. S4e_2,e_4) and cuboid (Fig. S4e_3) morphologies were observed in some cases. Irregular structure (Fig. S4c_2) and amorphous materials (Fig. S4a_4,d_4) had also been observed, in which cases the aggregates do not have any particular features. In the cases of $C_{12}AspNa_2$ + HTAB gels with 50, 60, and 80 wt% of HTAB exhibits fibrous, dense fibrous (Fig. S5a_1,b_1, and Table S1B) and densely-packed cuboid structures (Fig. S5c_1). $C_{12}GluNa_2$ + HTAB mixtures exhibit cuboid (Fig. S5a_2), irregular structures (Fig. S5b_2), and sheet-like structures (Fig. S5c_2)[27,28,57–59]. $C_{12}AspNa_2$ + HTAB and $C_{12}GluNa_2$ + HTAB gels show characteristic cuboid structures (Fig. S5c_1,a_2) due to the emergence of micropores at the surface of gels[60]. $C_{12}AspNa_2$ + HTAB gels have fibre network-like morphologies (Fig. S5a_1,b_1) that can hold water molecules due to assisted surface tension enhancement. Irregular (Fig. S5b_2) and sheet-like structures (Fig. S5c_2) for $C_{12}GluNa_2$ + HTAB indicate the entrapment of water molecules into the gels. Maximum number of HTAB accumulated in gels indicate that HTAB plays a fundamental role in demonstrating higher aggregation and formation of porous-like morphology, which are in consonance with the phase manifestation, and POM studies.

Phase transition and associated weight loss of gels were investigated by thermogravimetry analysis (TGA)[61–63]. Results on the TGA of the pure components, as well as AAS + HTAB aggregates, have been summarized in Fig. S6 and Table S2. HTAB decomposes to produce some solid carbon along with the production of long-chain hydrocarbon, nitrogen, and hydrogen[61,64], whereby decomposition of $C_{12}MalNa_2$, $C_{12}AspNa_2$ and $C_{12}GluNa_2$ to produce dodecane (or smaller alkyl fragments) and free aminomalonic, aspartic, and glutamic acid[63]. AAS + HTAB gels show endothermic peaks in the temperature range of 40 to 100 °C due to dehydration (Fig. 2a)[65]. Two carboxylate groups of $C_{12}MalNa_2$ electrostatically interact with HTAB that result in higher ionicity and subsequent moisture absorption capability than $C_{12}AspNa_2$ and $C_{12}GluNa_2$. In the case of $C_{12}GluNa_2$, two ionic carboxylate groups are separated by three methylene groups; so its interaction capability with HTAB and magnitude of hydration is lower. Formation of rigid aggregates result in the higher chain melting temperature (T_m) as determined from the DSC studies.

Thermotropic behaviour and associated parameters were evaluated by DSC studies[44]. Variation of phase transition temperature (T_m), width at half peak height ($\Delta T_{1/2}$), enthalpy change (ΔH) and corresponding heat capacity changes (ΔCp) were determined as functions of α_{AAS} as summarized in (Fig. 2). HTAB exhibits two endothermic peaks at 64 °C and 84 °C indicating transition from solid to liquid crystalline phase and the phenomenon

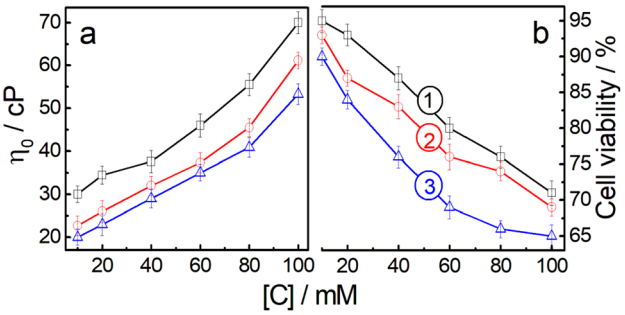

Figure 3. Variation of a, zero shear viscosity and b, human blood lymphocyte cell viability with AASs + HTAB (2/3, M/M) mixed surfactant concentration [C]. Systems: 1, $C_{12}MalNa_2$ + HTAB; 2, $C_{12}AspNa_2$ + HTAB and 3, $C_{12}GluNa_2$ + HTAB.

of dehydration[44], common in the amphiphiles (Fig. 2b)[63]. With increasing α_{AAS}, T_m values increase due to the incorporation of HTAB in the aggregates and assimilation of HTAB with AASs; relatively sharp peaks indicate favourable hydrocarbon chain packing (Fig. 2c)[49]. Lowering of T_m is due to size reduction, decreased specific surface area, and interaction between oppositely charged surfactants also known as Kelvin effect[66]. Widening of the melting peaks designates multi-crystallinity and heterogeneity[66]. The extent of hydrophobic interaction between AAS and HTAB is lower in $C_{12}AspNa_2$ and $C_{12}GluNa_2$, where the T_m values follow the sequence: $C_{12}MalNa_2$ + HTAB > $C_{12}AspNa_2$ + HTAB > $C_{12}GluNa_2$ + HTAB. With increasing α_{AAS}, $\Delta T_{1/2}$ values decrease indicating better packing of the hydrophilic overlayer as well as oppositely charged head groups (Fig. 2d). With increasing associative interaction between AAS and HTAB increased crystal imperfection results in higher $\Delta T_{1/2}$ values. Increasing magnitude of interaction with increasing proportion of HTAB induces the formation of ion-pair amphiphiles, resulting in higher ΔH values for the surfactant mixtures (Fig. 2e). With increasing α_{AAS}, ΔCp values gradually increase and exhibit endothermicity due to the formation of water overlayer around surfactant aggregates (Fig. 2f). Lower values of ΔCp are due to the increase in multicrystallinity.

Viscosity studies on AAS + HTAB mixtures at different combinations exhibit shear-thinning (results not shown)[49]. Zero shear viscosity (η_0) *vs.* concentration profile for the gels comprising 60 mol% HTAB are shown in Fig. 3a.

With increasing surfactant concentrations, viscosity increases monotonously in the range of 10 to 100 mM. The sequence in the viscosity variation follows the order: $C_{12}MalNa_2$ + HTAB > $C_{12}AspNa_2$ + HTAB > $C_{12}GluNa_2$ + HTAB, which are in consonance with the previous studies. Due to the stronger packing and subsequent formation of rigid-structured aggregates, the viscosity of $C_{12}MalNa_2$ + HTAB system is higher than the other two.

AAS + HTAB aggregates exhibit less toxicity against human blood lymphocyte up to 20 mM; although, cytotoxicity increases with increasing surfactant concentration (Fig. 3b). Results suggest that cytotoxicities are in consonance with the corresponding viscosity of the system.

Dermal responses towards the gels were assessed through topical application of the experimental gels on the bare mice skin surface where sterile distilled water and 5% (*w*/*v*) phenol-water were used as a negative (NC) and positive control (PC), respectively. Dermal irritability, as evidenced by the development of edema, and erythema were tested carefully and were scored according to the Organization for Economic Co-operation and Development (OECD) guidelines (Fig. 4A,C).

Simultaneously, developments of skin inflammation upon the application of gels were studied histologically by examining the hematoxylin-eosinY stained gel-treated skins for neutrophil invasion (Fig. 4B)[68,69]. It was found that gels do not induce symptoms related to skin irritation and inflammation (erythema, edema, and neutrophilic invasion) as shown in Fig. 4A(ii),B(ii). Effects of gels on mice skin appeared similar to the effect of sterile distilled water, used as negative control (NC). On the other hand, 5% (*w*/*v*) phenol-water (PC) caused considerable erythema, edema, and neutrophilic invasion Fig. 4A(iii),B(iii), resulting in high CII score (> 5.00) that corresponds to moderate skin irritation[67]. The CII score, for each of the gel treatment, was calculated to be as low as < 0.49 (Fig. 4C). These values, along with the CII values observed in NC group, correspond to the scores representing no potential skin irritation according to the OECD guidelines[67]. Besides, mice treated with 5% (*w*/*v*) phenol-water (PC group) visibly suffered from post-treatment erythema and edema resulting in higher CII score (> 5.00) that corresponds to moderate skin irritation[67]. Similarly, Fig. 4C reveals that there were significant differences ($P < 0.05$) in CII scores between 5% (*w*/*v*) phenol-water-treated group and each of the gel-treated groups. Based on these findings, it could be concluded that gels used in this study do not have significant skin irritation potential and thus may safely be used for topical dermal applications.

Gels also exhibited substantial antibacterial activities against *Staphylococcus aureus*, a gram-positive pathogenic bacteria. In spite of ~ 90% lymphocyte viability, 20 mM surfactant mixtures of AAS + HTAB (40:60, M/M) could substantially inhibit bacterial growth[67]. The minimum inhibitory concentration (MIC) is the lowest concentration of a substance that renders no turbidity in bacterial culture, corresponding to 99% bacterial growth inhibition[70]. The MIC value of individual surfactant mixture was determined for different clinical isolates of *S. aureus, i.e.*, American Type Culture Collection (ATCC) 25923 and four other clinical isolates: AK1, AK2, AK8, and AK10 with the broth dilution method. Vancomycin was also used as a reference drug for growth

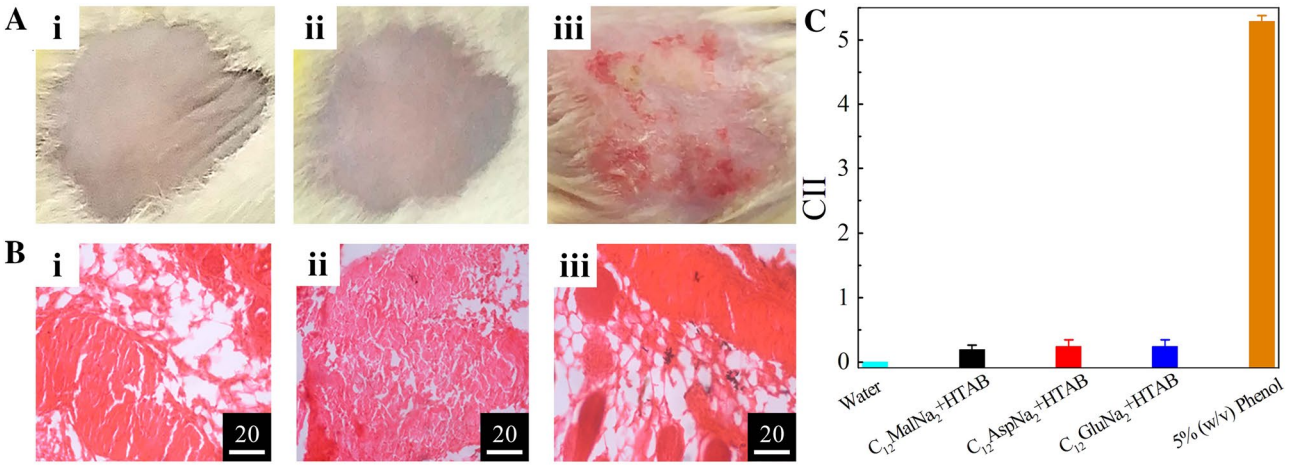

Figure 4. Effects of AAS + HTAB gels on mice skin. Gels were applied at the dorsal area of the trunk region of swiss albino mice for seven consecutive days and the effects recorded are presented through (**A**) photographs of treated skins and (**B**) corresponding histopathological evaluation of inflammation through micrographs. Systems: i, sterile distilled water (NC); ii, $C_{12}MalNa_2$ + HTAB gel (100 mM, 60/40, M/M) and iii, 5% (*w*/*v*) phenol-water (PC). Micrographic scale bar: 20 µm. (**C**) cumulative irritancy index (CII) scores for skins treated with different systems, calculated according to Organization for Economic Co-operation and Development (OECD) guidelines[67]. Overall comparison of CII scores among the groups were carried out by the Kruskal–Wallis test followed by post-hoc Dunn's test for multiple comparisons between each pair of groups. Significant differences in CII scores at $P < 0.05$ were obtained between groups PC *vs.* NC, PC *vs.* $C_{12}MalNa_2$ + HTAB, PC *vs.* $C_{12}AspNa_2$ + HTAB, and PC *vs.* $C_{12}GluNa_2$ + HTAB gels.

	MIC (µM)[a]			
***S.aureus* strains**	**Vancomycin**	**$C_{12}MalNa_2$ + HTAB**	**$C_{12}AspNa_2$ + HTAB**	**$C_{12}GluNa_2$ + HTAB**
AK1	0.827	20	40	20
AK2	1.242	40	60	40
AK8	1.035	40	50	40
AK0	0.827	30	40	30
ATCC 25923	0.482	10	20	10

Table 1. Antibacterial activities of AAS + HTAB gels against *S. aureus* clinical isolates. [a]For the determination of MIC value, serial concentrations in the range of 5 to 100 µM (with an increment of 5 µM in each step) of each surfactant mixture was applied to bacterial culture containing 1×10^7 CFU. Data represent mean values of three experimental outcomes.

inhibition[71,72] as it is a widely used effective 'drug of choice' against *S. aureus* infections[73]. With the MIC value in the range of 10–40 µM, $C_{12}MalNa_2$ + HTAB and $C_{12}GluNa_2$ + HTAB gels exhibited higher antibacterial activities than $C_{12}AspNa_2$ + HTAB, with the MIC value in the range of 20–60 µM, as summarized in Table 1.

Results indicate that gels can potentially be used in the treatment of bacteria-borne dermatological infections. In addition, the gels are expected to exhibit higher entrapment efficiency and sustained release of dermatological drugs in terms of topical applications. However, further in vitro and in vivo studies are warranted to substantiate the aptitude of the gels as potential drug delivery systems. Besides, studies involving composition structure and functional correlationships are also considered to be worthy.

Summary and conclusions

Microstructures of AAS + HTAB aggregates were investigated by combined phase manifestation, polarizing optical microscopy and field-emission scanning electron microscopic studies. Texture of liquid crystals depended on the concentration and proportion of constituent surfactants. Energetics of phase transition processes were evaluated by TGA and DSC studies. Cytotoxicity could be correlated with the viscosity of the gels. Gels impart insignificant skin irritation although they possess substantial antibacterial activities that project their potential as dermal drug delivery systems. However further in vitro and in vivo studies by incorporating appropriate drugs into the gels are necessary and is considered as the future perspectives.

In order to draw final conclusions about solvation, water channels, and pores, drawn from the morphological studies, further characterization techniques, viz., small-angle X-ray scattering and small-angle neutron scattering studies, combined with the molecular dynamics simulation studies are worthy to be investigated. These are considered as the future perspectives.

Experimental section

Materials. Hexadecyltrimethylammonium bromide (HTAB), fetal bovine serum (FBS) and histopaque-1077™ were the products from Sigma-Aldrich Chemicals Pvt. Ltd. (USA). Disodium salts of AAS were synthesized according to the previous reports[74]. Phenol, hematoxylin, eosin Y, and 3-(4, 5-dimethylthiazol-2-yl)-2, 5-diphenyl tetrazolium bromide (MTT) were purchased from Hi Media Laboratories Pvt. Ltd. India. Double distilled water was used throughout the experiments. All the chemicals were stated to be ≥ 99% pure and were used as received.

Methods. *Phase manifestation.* Composition, close to the boundary of the two-phase regions, was detected by homogeneous mixing of aqueous stock solution of oppositely charged surfactants at 25 °C. The exact boundary of the two-phase region was detected by further step wise addition (using a calibrated micropipette under constant stirring) of a higher concentration of AASs into the HTAB solution. On the basis of visual observation, more than one hundred samples were collected at different AASs and HTAB weight ratios and phase boundaries were identified[75]. The different phases were recorded consecutively for a longer time-period (upto fifteen days, after which the samples started microbial degradation). All the experiments were repeated thrice to ensure reproducibility.

Microscopic studies. The texture of different combinations of the mixed surfactant systems were recorded with a polarizing optical microscope (POM, Nikon ECLIPSELV100POL, Japan) set with a CCD camera. The sample was placed onto a glass slide and thereafter the POM images were recorded. Morphology of the surfactant aggregates were investigated with field emission-scanning electron microscopy (FE-SEM, ZEISS EVO 18, Germany). Samples were prepared by the drop-casting of the gel on a freshly cleaved mica foil and kept in air for two hours for solvent evaporation. Those were further dried at reduced pressure for two hours. The gold-sputtered samples were then analysed in FE-SEM at the operating voltage of 20–30 kV.

Thermogravimetric analysis (TGA). Weight loss and thermal stability of the gels were investigated by TGA, performed using Pyris 6 TGA-DTA-8000 (Perkin Elmer, USA). Samples were scanned in the temperature range of 50–500 °C with a scan rate of 2 °C min^{-1} under nitrogen gas flowing conditions.

Differential scanning calorimetric (DSC) studies. DSC studies were performed to evaluate the chain melting temperature (T_m) and associated thermodynamic parameters of mixed surfactant systems that control its physical states. DSC measurements were recorded using a Pyris 6 DSC-8000 (Perkin Elmer, USA) differential scanning calorimeter with indium as a calibrator before performing the experiment. After equilibrating for 10 min, the sample was scanned in the temperature range 0–100 °C with a scan rate of 2 °C min^{-1} during the heating cycle. From the thermogram the peak temperature and enthalpy of phase transition were evaluated. Endothermic peak *vs.* temperature in evaluating different physicochemical parameters of mixed surfactant system were considered[76].

Rheology studies. Viscosities of different surfactant mixtures were determined with a DV II-Pro rotoviscometer (Brookfield, USA) with a stated accuracy of ± 0.01 cP. 1.0 mL surfactant solution of different concentrations (40, 60, 80, and 100 mm) were taken in a cone and plate type rotoviscometer separately[77]. Viscosities were measured at different shear rates (ranging from 76 to 380 s^{-1}). Zero shear viscosity (η_0) was determined from the intercept of the plot of viscosity *vs.* shear rate by fitting polynomial regression. Temperature during the viscosity measurement was controlled by a circulatory water bath MIC-255 (Hanntech Corporation, South Korea).

Biological activities. All the biological experiments were performed in accordance with relevant guidelines and regulations, duly approved by the Institutional Ethics Committee, Vidyasagar University. All the methods were carried out in accordance with relevant guidelines and regulations.

Cytotoxicity studies. Cytotoxicity studies were carried out following the method of Sun et al.[67] 5 mL of human blood (volunteered by healthy persons) was diluted (1:1) with phosphate-buffered saline (PBS) and added to Histopaque-1077. Informed consent was obtained from all subjects. It was centrifuged at 1500 rpm for 40 min at the room temperature. The upper layer containing lymphocytes was further washed through centrifugation. Lymphocytes were re-suspended in Roswell Park Memorial Institute (RPMI) complete media supplemented with 10% (*w*/*v*) FBS and incubated for a day at 37 °C in 5% (*v*/*v*) CO_2 environment (in CO_2 incubator)[78]. Cytotoxicity of selected gels were estimated with MTT assay[79]. 20 µL 5% (*w*/*v*) MTT solution was added to each well of the microtitre plate, having RPMI-suspended lymphocytes with or without the gels. Then the plate was incubated at 37 °C for 4 h in metabolizing MTT to formazan. After the aspiration of the supernatant, 100 µL HCl + isopropanoic acid solution (1:1) was added to each well of the culture plate and mixed to dissolve the formazan crystals. Optical density (OD) of the sample was measured on an ELISA reader (Model 550, BIO-RAD, USA) using test and reference wavelengths of 570 and 630 nm, respectively. Percentage of cell viability was calculated using the following equation[79]:

$$\text{Cell viability } \% = \left[\text{OD}_{\text{sample}} - \text{OD}_{\text{control}}\right] \times 100/\text{OD}_{\text{control}} \quad (1)$$

Skin irritation test. The biocompatibility of the experimental gels (AAS + HTAB) were investigated through skin irritation tests on swiss albino mice, in compliance with the Animal Research: Reporting of in vivo Experiments (ARRIVE) guidelines[80]. The tests were performed following the method mentioned in the Good Laboratory Practice Standards (GLPS) manual and the guidelines of OECD for acute dermal irritation[81]. Thirty healthy swiss albino mice were divided into five groups, each group consisting of six mice. Group A was negative control (NC, treated with sterile distilled water) and group B was positive control (PC, treated with 5% (*w*/*v*) phenol-water). Mice of group C, D, and E were treated individually with 100 mM $C_{12}MalNa_2$ + HTAB, $C_{12}AspNa_2$ + HTAB and $C_{12}GluNa_2$ + HTAB gels, respectively. Prior to the application of gels, hairs of the dorsal area of the trunk region of all mice were removed followed by the topical application of 500 mL of the gels and the controls, respectively. After 1 h, signs of erythema or edema in individual animal was recorded. The entire procedure of dermal application of gels and subsequent recording for any irritation was continued for seven consecutive days. The CII score for each of the treated groups were calculated according to OECD guidelines[81]. CII score of each treated group is the average score, i.e., score of a total of erythema and edema divided by the number of animals and testing days.

Histological studies of mice skin. Animals were sacrificed post euthanasia by carbon dioxide asphyxiation after the completion of skin treatment with gels and controls for seven consecutive days. The treated skins were processed in wax blocks and transverse sections were prepared, followed by staining with hematoxylin-eosinY (HE)[69]. The prepared skin sections were further examined under a light microscope (Axioscope A1; Carl Zeiss, Germany). Histology of the gel-treated skins were compared with the controls.

Studies on antibacterial activity. Antibacterial efficacies of the gels against the gram-positive bacterial pathogen, *Staphylococcus aureus*, grown in Luria Bertani (LB) broth, were evaluated. MIC of each gel against the five clinical isolates of *S. aureus* (AK1, AK2, AK8 and AK10 along with ATCC 25923) was determined by broth dilution method. 10 µL gelatinous suspension of surfactant mixture at particular composition was added to 1 mL bacterial culture in LB having approximately 1×10^7 CFU. Each surfactant mixture (AAS + HTAB) was added to the bacterial culture in the concentration range of 5 to 100 µM (with an increment of 5 µM in each step) in a serial manner for individual bacteria and were incubated at 37 °C for 18 h[70–72,82]. Vancomycin was used as reference drug for growth inhibition. All the experiments were repeated thrice.

Statistical analysis. The mean value and standard deviation of the quantitative variables were calculated after repeating each quantification three times. Overall comparisons of data among the groups were carried out by the Kruskal–Wallis test. This was followed by post hoc Dunn's test for multiple comparisons of data between each pair of groups. Differences were considered significant at $P < 0.05$[83].

Received: 13 January 2021; Accepted: 16 June 2021
Published online: 30 July 2021

References

1. Fanasca, S. *et al.* Changes in antioxidant content of tomato fruits in response to cultivar and nutrient solution composition. *J. Agric. Food Chem.* **54**, 4319–4325 (2006).
2. Lopez-Leon, T., Fernandez-Nieves, A., Nobili, M. & Blanc, C. Nematic-smectic transition in spherical shells. *Phys. Rev. Lett.* **106**, 247802–247809 (2011).
3. Pelton, R. Temperature-sensitive aqueous microgels. *Adv. Colloid Interface Sci.* **85**, 1–33 (2000).
4. Saunders, B. R. & Vincent, B. Microgel particles as model colloids: Theory, properties and applications. *Adv. Colloid Interface Sci.* **80**, 1–25 (1999).
5. Williams, R. J. *et al.* Enzyme-assisted self-assembly under thermodynamic control. *Nat. Nanotechnol.* **4**, 19–25 (2009).
6. Barker, C. A., Saul, D., Tiddy, G. J. T., Wheeler, B. A. & Willis, E. Phase structure, nuclear magnetic resonance and rheological properties of viscoelastic sodium dodecyl sulphate and trimethylammonium bromide mixtures. *J. Chem. Soc. Farady. Trans.* **1**(70), 154–162 (1974).
7. Hammer, S. E., Ebert, M. & Weinbruch, S. Comparison of operator-and computer-controlled scanning electron microscopy of particles from different atmospheric aerosol types. *Anal. Bioanal. Chem.* **411**, 1633–1645 (2019).
8. Herrington, K. L., Kaler, E. W., Miller, D. D., Zasadzinski, J. A. & Chiruvolu, S. Phase behavior of aqueous mixtures of dodecyltrimethylammonium bromide (DTAB) and sodium dodecyl sulfate (SDS). *J. Phys. Chem.* **97**, 13792–13802 (1993).
9. Jokela, P., Jönsson, B. & Wennerström, H. Phase equilibria in systems containing both an anionic and a cationic amphiphile: A thermodynamic model calculation. *Surf. Ads. Surf. Spectr. Disp. Sys.* **235**, 17–22 (1985).
10. Sangeetha, N. M. & Maitra, U. Supramolecular gels: Functions and uses. *Chem. Soc. Rev.* **34**, 821–836 (2005).
11. Ohshima, H. (ed.) *Catanionic Surfactants: Novel Surrogates of Phospholipids* Vol. 1 (Wiley, 2016).
12. Holland, P. M. & Rubingh, D. N. Mixed surfactant systems, in mixed surfactant systems. *Am. Chem. Soc.* **114**, 2–30 (1992).
13. Kronberg, B. Surfactant mixtures. *Cur. Opin. Colloid Interface Sci.* **2**, 456–463 (1997).
14. Du, X., Zhou, J., Shi, J. & Xu, B. Supramolecular hydrogelators and hydrogels: From soft matter to molecular biomaterials. *Chem. Rev.* **115**, 13165–13307 (2015).
15. Hirst, A. R., Escuder, B., Miravet, J. F. & Smith, D. K. High-tech applications of self-assembling supramolecular nanostructured gel-phase materials: From regenerative medicine to electronic devices. *Angew. Chem.* **47**, 8002–8018 (2008).
16. Kato, T., Hirai, Y., Nakaso, S. & Moriyama, M. Liquid-crystalline physical gels. *Chem. Soc. Rev.* **36**, 1857–1867 (2007).
17. Matsumoto, S. *et al.* Photo gel–sol/sol–gel transition and its patterning of a supramolecular hydrogel as stimulited responsive biomaterials. *Chem. Eur. J.* **14**, 3977–3986 (2008).
18. Mizoshita, N., Kutsuna, T., Kato, T. & Hanabusa, K. Smectic liquid-crystalline physical gels: Anisotropic self-aggregation of hydrogen-bonded molecules in layered structures. *Chem. Commun.* **12**, 781–782 (1999).

19. Karsai, Á., Murvai, Ü., Soós, K., Penke, B. & Kellermayer, M. S. Oriented epitaxial growth of amyloid fibrils of the N27C mutant β25–35 peptide. *Eur. Biophys. J.* **37**, 1133–1137 (2008).
20. Li, Z. *et al.* Observation of exchange bias in the martensitic state of $Ni_{50}Mn_{36}Sn_{14}$ Heusler alloy. *Appl. Phys. Lett.* **91**, 112505 (2007).
21. Chivers, P. R. & Smith, D. K. Shaping and structuring supramolecular gels. *Nat. Rev. Mater.* **4**, 463–478 (2019).
22. Ding, R. *et al.* Hybrid photosensitizer based on amphiphilic block copolymer stabilized silver nanoparticles for highly efficient photodynamic inactivation of bacteria. *RSC Adv.* **6**, 20392–20398 (2016).
23. Krall, A. H. & Weitz, D. A. Internal dynamics and elasticity of fractal colloidal gels. *Phys. Rev. Lett.* **80**, 778–781 (1998).
24. Li, L. *et al.* A nanostructured conductive hydrogels-based biosensor platform for human metabolite detection. *Nano Lett.* **15**, 1146–1151 (2015).
25. Pan, L. *et al.* Hierarchical nanostructured conducting polymer hydrogel with high electrochemical activity. *Proc. Natl. Acad. Sci.* **109**, 9287–9292 (2012).
26. Zhai, D. *et al.* Highly sensitive glucose sensor based on Pt nanoparticle/polyaniline hydrogel heterostructures. *ACS Nano* **7**, 3540–3546 (2013).
27. Cornwell, D. J., Okesola, B. O. & Smith, D. K. Multidomain hybrid hydrogels: spatially resolved photopatterned synthetic nanomaterials combining polymer and low molecular weight gelators. *Angew. Chem.* **126**, 12669–12673 (2014).
28. de Jong, J. J. *et al.* Light driven dynamic pattern formation. *Angew. Chem.* **44**, 2373–2376 (2005).
29. Draper, E. R., Eden, E. G., McDonald, T. O. & Adams, D. J. Spatially resolved multicomponent gels. *Nat. Chem.* **7**, 848 (2015).
30. Eastoe, J., Sánchez-Dominguez, M., Wyatt, P. & Heenan, R. K. A photo-responsive organogel. *Chem. Commun.* **14**, 2608–2609 (2004).
31. Nolan, M. C. *et al.* Optimising low molecular weight hydrogels for automated 3D printing. *Soft Mater.* **13**, 8426–8432 (2017).
32. Wei, Q. *et al.* Printable hybrid hydrogel by dual enzymatic polymerization with superactivity. *Chem. Sci.* **7**, 2748–2752 (2016).
33. Raeburn, J. *et al.* Electrochemically-triggered spatially and temporally resolved multi-component gels. *Mat. Horizons* **1**, 241–246 (2014).
34. Inostroza-Brito, K. E. *et al.* Co-assembly, spatiotemporal control and morphogenesis of a hybrid protein-peptide system. *Nat. Chem.* **7**, 897 (2015).
35. Olive, A. G. *et al.* Spatial and directional control over self-assembly using catalytic micropatterned surfaces. *Angew. Chem.* **53**, 4132–4136 (2014).
36. Rodon, F. *et al.* Localized supramolecular peptide self-assembly directed by enzyme-induced proton gradients. *Angew. Chem.* **129**, 16200–16204 (2017).
37. Hu, B. *et al.* Supramolecular hydrogels for antimicrobial therapy. *Chem. Soc. Rev.* **47**, 6917–6929 (2018).
38. Okesola, B. O. & Smith, D. K. Applying low-molecular weight supramolecular gelators in an environmental setting-self-assembled gels as smart materials for pollutant removal. *Chem. Soc. Rev.* **45**, 4226–4251 (2016).
39. Weiss, Richard G., Molecular gels : structure and dynamics, Monographs in supramolecular chemistry, no. 25., Cambridge : Royal Society of Chemistry (2018)
40. Bordes, R., Tropsch, J. & Holmberg, K. Counterion specificity of surfactants based on dicarboxylic amino acids. *J. Colloid Interface Sci.* **338**, 529–536 (2009).
41. Pinazo, A., Pons, R., Pérez, L. & Infante, M. R. Amino acids as raw material for biocompatiable surfactants. *Ind. Eng. Chem. Res.* **50**, 4805–4817 (2011).
42. Nakata, K., Tsuchido, T. & Matsumura, Y. Antimicrobial cationic surfactant, cetyltrimethylammonium bromide, induces superoxide stress in *Escherichia coli* cells. *J. Appl. Microbiol.* **110**, 568–579 (2011).
43. Hrenovic, J. & Ivankovic, T. Toxicity of anionic and cationic surfactant to *Acinetobacter junii* in pure culture. *Open Life Sci.* **2**, 405–414 (2007).
44. Maiti, K., Bhattacharya, S. C., Moulik, S. P. & Panda, A. K. Physicochemical studies on ion-pair amphiphiles: Solution and interfacial behaviour of systems derived from sodium dodecylsulfate and n-alkyltrimethylammonium bromide homologues. *J. Chem. Sci.* **122**, 867–879 (2010).
45. Li, J.-L. & Liu, X.-Y. Microengineering of soft functional materials by controlling the fiber network formation. *J. Phys. Chem. B* **113**, 15467–15472 (2009).
46. Li, S. *et al.* Synthesis and thermoelectric properties of the new oxide materials $Ca_{3-x}Bi_xCo_4O_9+\delta$ ($0.0< x< 0.75$). *Chem. Mater.* **12**, 2424–2427 (2000).
47. Herwig, P., Kayser, C. W., Müllen, K. & Spiess, H. W. Columnar mesophases of alkylated hexa-peri-hexabenzocoronenes with remarkably large phase widths. *Adv. Mater.* **8**, 510–513 (1996).
48. Aouini, A. *et al.* Chemical-physical characterization of a binary mixture of a twist bend nematic liquid crystal with a smectogen. *Curr. Comput. Aided Drug Des.* **10**, 1110 (2020).
49. Barai, M. *et al.* Interfacial and aggregation behavior of dicarboxylic amino acid based surfactants in combination with a cationic surfactant. *Langmuir* **35**, 15306–15314 (2019).
50. Maréchal, J.-P., Matsumura, K., Conlan, S. & Hellio, C. Competence and discrimination during cyprid settlement in *Amphibalanus amphitrite*. *Int. Biodeterior. Biodegrad.* **72**, 59–66 (2012).
51. van der Kooij, F. M. & Lekkerkerker, H. N. Formation of nematic liquid crystals in suspensions of hard colloidal platelets. *J. Phys. Chem. B* **102**, 7829–7832 (1998).
52. Fan, S. R., Willis, P. C. & Clark, N. A. The field induced stripe texture in surface stabilized ferroelectric liquid crystal cells. *Ferroelectrics* **121**, 127–136 (1991).
53. Kokini, J. L., Kadane, J. B. & Cussler, E. L. Liquid texture perceived in the mouth1. *J. Texture Struct.* **8**, 195–218 (1977).
54. Haas, W. E. & Adams, J. E. Electrically variable diffraction in spherulitic liquid crystals. *Appl. Phys. Lett.* **25**, 263–264 (1974).
55. Bag, B. G., Hasan, S. N., Pongpamorn, P. & Thasana, N. First hierarchical self-assembly of a seco-triterpenoid α-onocerin yielding supramolecular architectures. *Chem. Select* **2**, 6650–6657 (2017).
56. Criado-Gonzalez, M. *et al.* Enzyme-assisted self-assembly within a hydrogel induced by peptide diffusion. *Chem. Commun.* **55**, 1156–1159 (2019).
57. Bhattacharya, S. & Acharya, S. G. Pronounced hydrogel formation by the self-assembled aggregates of N-alkyl disaccharide amphiphiles. *Chem. Mater.* **11**, 3504–3511 (1999).
58. Datta, S. & Bhattacharya, S. Multifarious facets of sugar-derived molecular gels: molecular features, mechanisms of self-assembly and emerging applications. *Chem. Soc. Rev.* **44**, 5596–5637 (2015).
59. Piras, C., Slavik, P. & Smith, D. K. Self-assembling supramolecular hybrid hydrogel beads. *Angew. Chem.* **34**, 567–571 (2014).
60. Uva, M. & Atrei, A. Surface morphology at the microscopic scale, swelling/deswelling, and the magnetic properties of PNIPAM/CMC and PNIPAM/CMC/Fe_3O_4 hydrogels. *Gels* **2**, 30–34 (2016).
61. Mukherjee, A. *et al.* Gold-catalyzed 1, 2-difunctionalizations of aminoalkynes using only N-and O-containing oxidants. *J. Am. Chem. Soc.* **133**, 15372–15375 (2011).
62. Sui, L., Wang, F. & Li, B. Adult-onset hypothyroidism impairs paired-pulse facilitation and long-term potentiation of the rat dorsal hippocampo-medial prefrontal cortex pathway in vivo. *Brain Res.* **1096**, 53–60 (2006).
63. Varughese, P., Saban, K., George, J., Paul, I. & Varghese, G. Crystallization and structural properties of calcium malonate hydrate. *J. Mater. Sci.* **39**, 6325–6331 (2004).

64. Xia, Y., Tse, C. & Lau, F.C.-M. Performance of differential chaos-shift-keying digital communication systems over a multipath fading channel with delay spread. *IEEE Trans. Circuits Syst. II Express Briefs* **51**, 680–684 (2004).
65. Weiss, I. M., Muth, C., Drumm, R. & Kirchner, H. O. Thermal decomposition of the amino acids glycine, cysteine, aspartic acid, asparagine, glutamic acid, glutamine, arginine and histidine. *BMC Biophys.* **11**, 2–7 (2018).
66. Nahak, P. *et al.* Influence of lipid core material on physicochemical characteristics of an ursolic acid-loaded nanostructured lipid carrier: An attempt to enhance anticancer activity. *Langmuir* **32**, 9816–9825 (2016).
67. Sun, M.-L. *et al.* Characterization and biotechnological potential analysis of a new exopolysaccharide from the arctic marine bacterium *Polaribacter* sp. SM1127. *Sci. Rep.* **5**, 18435–18441 (2015).
68. Jemal, A. *et al.* Cancer statistics. *CA Cancer J. Clin.* **57**, 43–66 (2007).
69. Agbaje, T., Mondal, S., Makukula, Z., Motsa, S. & Sibanda, P. A new numerical approach to MHD stagnation point flow and heat transfer towards a stretching sheet. *Ain Shams Eng. J.* **9**, 233–243 (2018).
70. Karmakar, A., Jana, D., Dutta, K., Dua, P. & Ghosh, C. Prevalence of panton-valentine leukocidin gene among community acquired *Staphylococcus aureus*: A real-time PCR study. *J. Pathog.* **2**, 245–249 (2018).
71. Dutta, K. *et al.* Benzyl isocyanate isolated from the leaves of Psidium guajava inhibits *Staphylococcus aureus* biofilm formation. *Biofouling* **36**, 1000–1017 (2020).
72. Karmakar, A., Dua, P. & Ghosh, C. Biochemical and molecular analysis of Staphylococcus aureus clinical isolates from hospitalized patients. *Can. J. Infect. Dis. Med. Microbiol.* **9041636**, 24–29 (2016).
73. McGuinness, W. A., Malachowa, N. & DeLeo, F. R. Vancomycin resistance in *Staphylococcus aureus*. *J. Biol. Med.* **90**, 269–281 (2017).
74. Bordes, R. & Holmberg, K. Physical chemical characteristics of dicarboxylic amino acid-based surfactants. *Colloids Surf. A* **391**, 32–41 (2011).
75. Kaler, E. W., Herrington, K. L., Murthy, A. K. & Zasadzinski, J. A. Phase behavior and structures of mixtures of anionic and cationic surfactants. *J. Phys. Chem.* **96**, 6698–6707 (1992).
76. Choffat, F. *et al.* Synthesis and characterization of linear poly (dialkylstannane). *Macromolecules* **40**, 7878–7889 (2007).
77. Sastry, N. V. & Singh, D. K. Surfactant and gelation properties of acetylsalicylate based room temperature ionic liquid in aqueous media. *Langmuir* **32**, 10000–10016 (2016).
78. Preston, K. L., Bigelow, G. E., Bickel, W. K. & Liebson, I. A. Drug discrimination in human postaddicts: Agonist-antagonist opioids. *J. Pharm. Exp. Therap.* **250**, 184–196 (1989).
79. Weichert, A. & Hoffmann, H. M. R. Synthesis and reactions of alpha-methylene-beta-keto sulfones. *J. Org. Chem.* **56**, 4098–4112 (1991).
80. du Sert, N. P. *et al.* The ARRIVE guidelines 2.0: Updated guidelines for reporting animal research. *PLOS Biol.* **18**, 3000410–3000417 (2020).
81. OECD, Test No. 404: Acute Dermal Irritation/Corrosion, OECD Publishing, Paris (2002)
82. Sufian, A. & Russell, A. R. Microstructural pore changes and energy dissipation in Gosford sandstone during pre-failure loading using X-ray CT. *Int. J. Rock Mech. Min. Sci.* **57**, 119–131 (2013).
83. Biswas, S. *et al.* Quorum sensing auto inducer (s) and flagellum independently mediate EPS signaling in *Vibrio cholerae* through luxo-independent mechanism. *Microbiol. Ecol.* **77**, 616–630 (2019).

Acknowledgements

This work has been financially supported by University Grants Commission (UGC), New Delhi, India through a UGC-BSR Scheme, (F.25-1/2014-15(BSR)/7-234/2009(BSR) UGC-SAP (No. F. 5-9/2015/DRS-II (SAP-II) and Department of Science and Technology, Govt. of India, New Delhi, India through the DST-FIST grants (No. SR/FST/CS-I/2017/7 (C).

Author contributions

MB, EM, HS and MKM studied the physicochemical properties KCG, TM and CG studied the biological activities AP and AL synthesized the anionic surfactants PM studied the DSC and TGDTA CC, CG, AKP and SB prepared the manuscript.

Competing interests

The authors declare no competing interests.

Additional information

Supplementary Information The online version contains supplementary material available at https://doi.org/10.1038/s41598-021-94777-2.

Correspondence and requests for materials should be addressed to A.K.P.

Reprints and permissions information is available at www.nature.com/reprints.

Publisher's note Springer Nature remains neutral with regard to jurisdictional claims in published maps and institutional affiliations.